CORA Cork Open Research Archive
Cartlann Taighde Oscailte Chorcaí

Title	Surface morphology evolution of AlGaN microhoneycomb structures during epitaxial overgrowth
Authors	Singh, Sandeep M.;Zubialevich, Vitaly Z.;Parbrook, Peter J.
Publication date	2024-01-07
Original Citation	Singh, S. M., Zubialevich, V. Z. and Parbrook, P. J. (2024) 'Surface morphology evolution of AlGaN microhoneycomb structures during epitaxial overgrowth', physica status solidi (b), 261(3), 2300471 (13pp). https://doi.org/10.1002/pssb.202300471
Type of publication	Article (peer-reviewed)
Link to publisher's version	10.1002/pssb.202300471
Rights	© 2023 Wiley-VCH GmbH. This is the accepted version of the following item: Singh, S. M., Zubialevich, V. Z. and Parbrook, P. J. (2024) 'Surface morphology evolution of AlGaN microhoneycomb structures during epitaxial overgrowth', physica status solidi (b) – basic solid state physics, 2300471 (13pp), which has been published in final form at: https://doi.org/10.1002/pssb.202300471 This article may be used for non-commercial purposes in accordance with Wiley Terms and Conditions for Use of Self-Archived Versions.
Download date	2026-09-15 04:50:06
Item downloaded from	https://hdl.handle.net/10468/15410

UCC
University College Cork, Ireland
Coláiste na hOllscoile Corcaigh

Surface Morphology Evolution of AlGaN Micro-Honeycomb Structures during Epitaxial Overgrowth

Sandeep M. Singh[1, 2], Vitaly Z. Zubialevich[1*] and Peter J. Parbrook[1, 2]

[1] *Tyndall National Institute, University College Cork, Cork, Ireland*

[2] *School of Engineering, University College Cork, Cork, Ireland*

* *Corresponding author: vitaly.zubialevich@tyndall.ie*

The surface morphological development during epitaxial overgrowth of AlGaN on micro-honeycomb (µ-HC) patterned relaxed AlGaN/AlN/sapphire templates is studied. Optimisation of µ-pattern design and influence of various growth parameters were carried out in search for conditions resulting in coalescence of µ-HC structures into planar layers or ordered arrays of V-pits with well-defined crystallographic facets. It was found that in a wide range of growth conditions, formation of V-pits with semi-polar facets occurs where their crystallographic orientation is defined by the geometry of the initial µ-HC patterns and growth conditions. High temperature and high V/III ratio conditions were found to favour *c*-plane expansion and allow recovery of planarity on the patterned templates. Systematic study of surface morphology evolution in conditions favouring a) semi-polar facets formation and b) coalescence was carried and possible mechanisms underpinning the observed behaviours have been proposed.

Introduction:

Aluminium gallium nitride (AlGaN) based UV LEDs emitting in the range of 300-350 nm require AlGaN buffer layers with aluminium content of ≤ 50% which are crack-free, transparent and of low threading dislocation density. Generally, for UV LEDs at longer and shorter operating

wavelength, binary compound buffer layers can be grown as a template on cost effective substrate such as sapphire. Strain and dislocation engineering techniques[1–8] can allow good crystal quality for device overgrowth. However, strain issues preclude this approach at these intermediate wavelengths: direct growth of $Al_{x<0.5}Ga_{1-x}N$ on either GaN or AlN single crystal substrates does not generally lead to good results. Generation of cracks due to the tensile stress in the former case and significant quality deterioration via surface morphology degradation and plastic relaxation through dislocation formation because of strong compressive stress in the latter case makes the use of direct growth on AlN or GaN templates unpractical. This unfortunate circumstance makes it hard to get UVB LEDs with decent efficiencies and partly explains superiority of UVA and even some ranges of UVC LEDs over UVB ones (Fig. 1.3 in Ref. [9]).

As a result of the challenges in finding a template with manageable strain, templates for 300-350 nm LEDs tend to have high densities of threading dislocations. Such threading dislocations impede the optical quality[10–12] and electrical performance[13] of the material. Furthermore, such highly dislocated AlGaN is susceptible to cracking when doped with silicon to achieve *n*-type which limits achievable thicknesses of the *n*-AlGaN buffer layers[6].

To address the above problems a number of techniques were employed, such as low temperature interlayers[7], superlattices[6], SiN_x interlayers[8]. Due to the high stickiness, of aluminium adatoms and thus difficulties in implementing selective area growth approaches, the most promising dislocation filtering techniques for AlGaN are those based on patterning (on nano- or microscale) of typical quality heteroepitaxially grown layers and their consequent coalescence back into planar ones by overgrowth[1–5]. Allerman *et al.*[3] patterned AlGaN into arrays of long strips, overgrew them with several micron thick AlGaN until complete coalescence, and obtained reduced TDDs. However, the anisotropic shape of the 1D structures leads to non-uniform distribution of strain (different strain along the direction of strips and perpendicular to their direction), which in its turn can lead to undesired cracking[2,14]. Nano- and micropatterning in 2D should eliminate this issue. Omori *et al.*[4] demonstrated improved quality crack-free Al-rich AlGaN by overgrowth on top of triangular arrays

of AlN nanopillars. Regrowth of such incoherent regions as nanopillars very much rely on the quality of the initial (before patterning) templates due to otherwise strong mutual tilt and twist of isolated from each other regions which results in additional dislocations in the coalesced layer. For this reason, nanopatterning of AlGaN into structures preserving the coherence across full wafer might be more promising.

On the other note, it is important to study the range of growth conditions to understand which of them allow coalescence of patterned structures, which do not, and why. Most of the previous studies lack this analysis and focused more on dislocation reduction aspect and not on growth mechanisms leading to different surface morphology evolutions.

In this work, we present results of $Al_{\sim 0.2}Ga_{\sim 0.8}N$ overgrowth on relaxed (i.e. of typical achievable quality for planar material: DD of the order of mid-high 10^9 cm^{-2}) AlGaN/AlN/sapphire templates patterned on microscale with 2D arrays of hexagonal holes. We study the effect of various growth parameters on the surface morphology evolution of such microhoneycomb (μ-HC) structures which preserve the overall coherence of the material across full wafer.

The initial aim of this study was to find conditions suitable for *c*-plane expansion and coalescence of the μ-HC structures into planar layers. When it became clear that across a wide range of growth parameters it is possible to obtain structures with semi-polar facets, additional efforts were directed towards identifying conditions resulting in well-defined crystallographically regular arrays of such V-pits. The effects of reactor pressure, V/III ratio, carrier gas and substrate temperature on surface morphology of the resulting structures were studied for samples with different orientations of the hexagonal array relative to crystallographic orientation of the initial AlGaN/AlN/sapphire templates. The observed behaviours are then explained based on mechanisms taking into consideration growth rate ratio along different crystallographic orientations.

1 Experimental

Initial planar AlGaN templates were grown by metal organic chemical vapour deposition (MOCVD) in a showerhead type vertical flow 3×2” Aixtron MOCVD reactor using trimethylgallium,

trimethylaluminum and ammonia as precursors. The growth was carried out in hydrogen ambient starting from 200 nm AlN connecting layer on commercial sapphire substrates with thin AlN nucleation layer (Kyma Technologies). Standard growth conditions (75 mbar, 1060°C, NH_3: ~10% of total flow which corresponds to V/III ratio of ~200) were then used to grow ~2 µm of nominally undoped $Al_{\sim 0.2}Ga_{\sim 0.8}N$.

The samples were then characterized by Panalytical X-pert MRD X-ray diffraction system using symmetric (002) ω-scan and skew-symmetric (101) ω-scan to determine the screw and edge type dislocation density. As a result, a typical for planar growth quality (total dislocation density of about $3\text{-}4\times10^9$ cm^{-2}) was achieved with most dislocations being of edge type.

Standard optical photolithography and metal lift-off process were then used to create palladium hard mask in the form of hexagonal arrays of circular holes (~2 µm in diameter with 3 µm pitch) in the metal on top of AlGaN epilayers preliminarily capped with a thin layer of SiO_2. Using inductively coupled plasma (ICP) dry etch (Oxford Instruments PlasmaPro Cobra ICP etcher, Cl_2 chemistry (50 sccm), RF/ICP powers of 100 W/1200 W, 7.5 mTorr, 20°C), the holes in the hard mask were translated into AlGaN forming nearly cylindrical cavities into it (Figure 1. *a* and *e*).

After elimination of palladium hard mask residuals in aqua regia, to remove also ICP-damaged AlGaN and further expand the holes, a wet etch with a hot KOH-based solution (AZ400K) was used. While the thin SiO_2 layer was attacked and ultimately removed by the wet etch, it is believed that its presence improves homogeneity of the expansion. The wet etch transforms circular holes into hexagonal ones due its anisotropic nature: *m*-oriented {1$\underline{1}$00} facets appear to be slowest etched among a variety of non-polar orientations present in the circular holes. The hexagonal shape of the holes after the wet etch defines two possible arrangements of arrays relative to crystallographic orientation of AlGaN: hexagons facing their neighbour's corner to corner where triangular regions appear in between three neighbouring hexagons (Figure 1, *b*, *f*) or side to side so that sidewalls of the hexagon form 'Y' letters (Figure 1, *d*, *h*). We refer to these two distinct µ-HC patterns as Δ- and Y-type respectively.

The duration of the wet etch allows to control the lateral dimension of the µ-holes and thus the amount of removed material. Particularly, in the case of Δ-type array, a prolonged etch time resulted in disjointed triangular regions (Figure 1, *c*, *g*); we will refer this sample as Δ+-type.

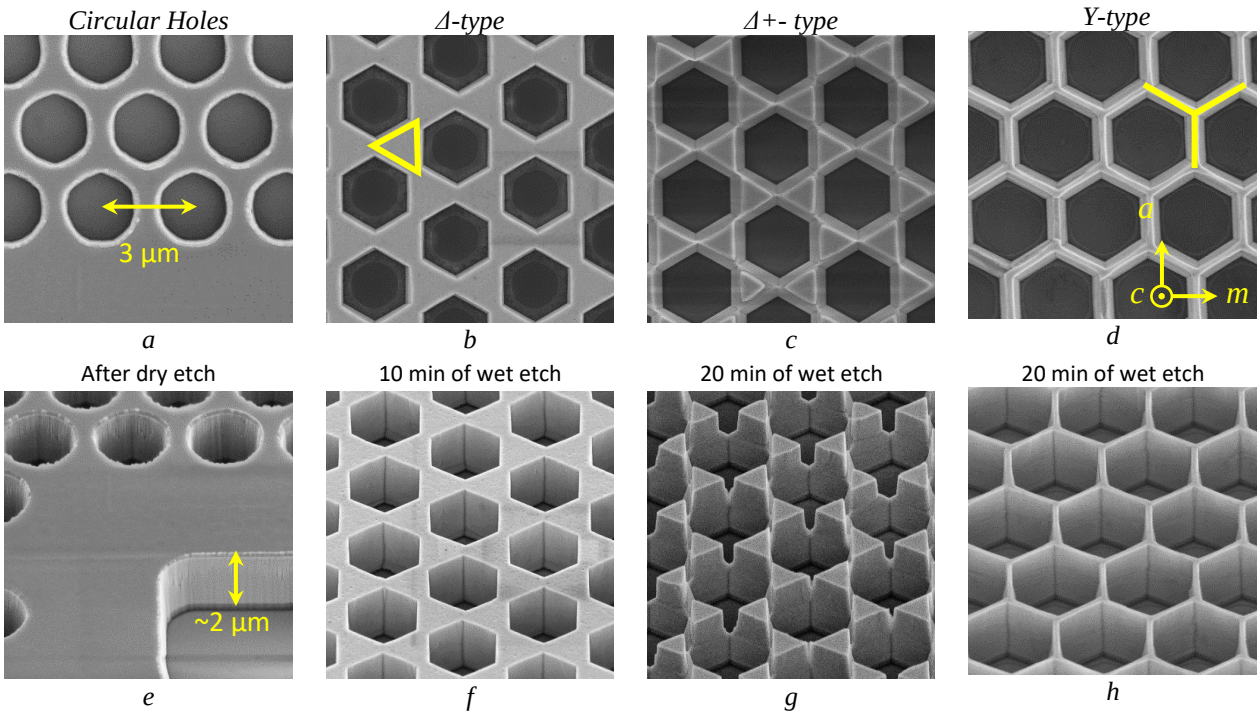

Figure 1. – Top view (a-d) and 45° tilted view (e-h) SEM images of AlGaN layers patterned into µ-HC: (a, e) - after dry etch; (b, f) - after 10 min wet etch in hot AZ (Δ-type); (c, g) - after 20 min wet etch in hot AZ (Δ+-type); and (d, h) - after 20 min wet etch in hot AZ (Y-type). The array pitch for all samples is fixed at 3 µm.
Here and below: the width of the images is 9.2 µm unless specified otherwise; crystallographic orientation of AlGaN array as specified in image (d)

These µ-patterned structures were then used for series of overgrowth experiments to study the surface morphology at different growth conditions. The same approach was used for overgrowth as for the growth of initial planar templates described above.

AlGaN overgrown samples were characterized by scanning electron microscopy using Carl Zeiss Supra 40 and FEI Quanta 650 FEG to access their surface morphology.

2 Results and Discussions

2.1 GaN overgrowth

Initially, a series of test growths of GaN on Δ-type samples using standard GaN conditions (1060°C, 150 mbar, NH_3: 33% of total flow, which corresponds to V/III ratio of ~1000) was undertaken to study the evolution of surface morphology. This experiment resulted in a

straightforward *c*-plane expansion and complete coalescence of µHC structure into planar layer within ~2.5 µm of total growth (Figure 1 in Supplementary Information). This result is rather expected as exactly these conditions are used in standard GaN on sapphire growth after annealing the low temperature nucleation layer (NL)[15] and lead to coalescence of NL islands into planar layers.

These GaN conditions were used as a starting point for our study of AlGaN overgrowth since the main aim of this study initially was to coalesce µ-HC, and our target material contains only about 20% of nominal (corresponding to that in a planar reference sample) aluminium content.

It should be noted in this regard that concerning µ-HC structures, one can only speculate about nominal Al-content as different crystallographic orientations present during different stages of overgrowth will be strictly saying of different Al-content. During growth, they compete for precursors, and this competition is affected by properties of Ga- and Al-adatoms in terms of diffusion lengths and stickiness coefficients, which besides growth parameters also depend on crystallographic orientation of AlGaN surface.

2.2 AlGaN overgrowth using standard GaN conditions

When an attempt to implement the above growth conditions was undertaken to deposit 2 µm of AlGaN (on a planar reference wafer co-loaded together with a patterned sample), no coalescence was observed, and instead hexagonal in base V-pits were formed with well-defined crystallographic semipolar facets (Figure 2) with almost complete disappearance of the original *c*-plane. The formation of semipolar facets occurs as a result of competition between pluralities of crystallographic orientation present in the initial µ-HC. While detailed data on surface evolution will be presented later, it is worth noting already now that growth initiates along *c*-plane

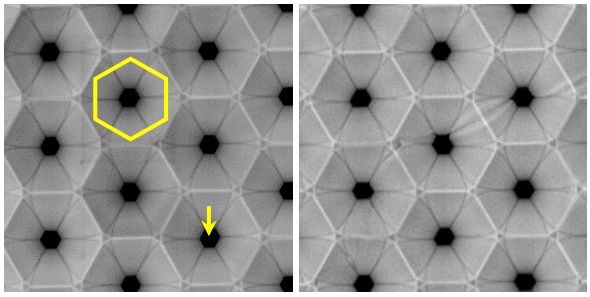

a *b*

Figure 2: SEM images of (a) Δ- and (b) Δ+-type samples after growth of ~2 µm AlGaN at 1060°C and 150 mbar in high V/III ratio. The yellow hexagon in figure (a) shows the orientation of µ-hole base prior to growth. The arrow points to the part of a V-pit, which is referred in the main text as 'tunnel' region.

and non-polar planes. A semipolar plane appearing in between them can indicate its relatively slow growth rate. This can be better understood from consideration of Figure 3.

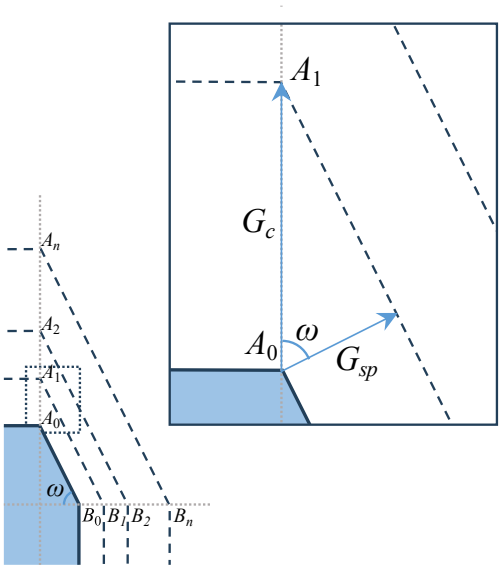

Figure 3. – Schematic of one possible surface evolution of a µ-HC sidewall where its initial top horizontal c-plane facet neither expands nor shrinks. Material of the µ-HC sidewall is represented in light blue colour.

For an arbitrary structure with pre-existing three facets: polar, semi-polar and non-polar, to preserve its shape i.e. points $A_{i>0}$ stay at the same x as the initial point A_0 and points $B_{j>0}$ stay at the same y as the initial point B_0, the growth rate ratios along these three directions should be in the following relations with each other:

$$G_c \cos(\omega) = G_{sp} = G_{np} \sin(\omega), \quad (1)$$

where G_c, G_{sp} and G_{np} are the growth rates along c-, semi-polar and non-polar planes, respectively, and ω is the angle between the semi-polar and c-planes. In the case of the semi-polar plane growth rate G_{sp} being larger than both left and right sides of equation (1), its area will shrink (or will not appear if it did not pre-exist as in our case). This is not what is observed in our experiment (Figure 2), and therefore, the opposite relation should take place confirming our postulation of slow semi-polar plane growth rate made in the previous paragraph.

From the same considerations, it is also clear that coalescence can be achieved when points $A_{i>0}$ move to the right relative to the initial point A_0, i.e.,

$$G_{sp}/G_c > \cos(\omega) \quad (2)$$

From a cross-section SEM measurement (not shown), the angle of the semipolar facets was found to be close to 60° with respect to the c-plane. This means that to achieve coalescence, we need to identify growth conditions at which the growth rate along the semipolar facet is faster than approximately a half of growth rate along c-plane.

On another note, from the angle between semipolar facets and *c*-planes being ~60° we can speculate that their crystallographic orientations should be either from the {1101} or {1122} of planes (theoretical values of 62° and 58°, respectively[16]). From comparison, for example, of Figure 1, *c* and Figure 2, *a*, it is clear that they are {1122} planes as the orientation of the hexagon rotates by 30° after growth (as was noted early, the original µ-HC holes had almost vertical i.e. nearly *m*-plane sidewalls).

Without going into detail, the rotation of hexagons after growth is defined by the ratio between growth rates along competing semipolar facets. For growth in apertures, the *dominant* planes are those that are faster growing. Based on considerations analogous to those we introduced while discussing Figure 3 and considering the competition between {1101} and {1122} facets, it is possible to show that growth rate along 11$\underline{2}$2 needs to be faster by approx. 1.155 (1/cos(30°)[*] for this twist to happen. So, while as it will be shown later this is not always the case, we have to conclude that in these growth conditions this requirement is satisfied which is why this transformation takes place.

On the final note to these results, it is worth to mention that some imperfections and irregularities are observed for the Δ+ sample (Figure 2, *b*) grown in the same run which suggest that disjointed patterns will require more time to develop a uniform semipolar regions or will have a hard time to converge into a uniform regular structure.

Despite the promising results in terms of realising such novel faceted structures, AlGaN growth using the standard GaN conditions appears to be not optimal because of the requirement to apply a high trimethyl-aluminium (TMAl) to trimethyl-gallium ratio in the gas phase to the reach the aluminium content in the solid around 20% (our target). As another result of the significant pre-reaction of trimethyl-aluminium with ammonia[17], a heavy deposition of white particles (most

[*] This rough estimation is based on hexagonal geometry of the initial µ-holes. Here, we consider the ratio of the distance from the hexagon apexes to the µ-hole centre to the lateral component of growth rate along *a*-plane tilted facets {11$\underline{2}$2}. This time is then compared to the ratio of the distance from the middle of hexagon side to the µ-hole centre to the lateral component of growth rate along *m*-plane tilted facets {1$\underline{1}$01}. For simplicity, we assume that both of these semipolar facet families are tilted by ~60° from the *c*-plane. It is considered that the plane that reaches the centre of µ-hole earlier will become the dominant plane. A more precise analysis considering the individual (for each plane family) tilt angles gives a factor of 1.114 instead of the above mentioned 1.155.

probably AlN or high aluminium content AlGaN) on the quartz parts of the reactor was observed. Lowering growth pressure is one of the ways to reduce the unwanted pre-reaction and utilize precursors more efficiently. From these considerations, the effect of reduction of pressure was evaluated.

2.3 Effect of low pressure

While reducing pressure can suppress the unwanted pre-reaction of TMAl with ammonia[17], the reduced pre-reaction will increase the growth rate (with more aluminium incorporating) and thus the aluminium content of AlGaN. To bring it back to the original ~20%, the TMAl/TMGa ratio was reduced accordingly. Figure 4 shows µ-HC sample grown at the reduced growth pressure of 75 mbar.

Comparing Figure 2, *a* and Figure 4 one can see that no significant impact of pressure reduction on the surface morphology takes place. Based on this finding and in order to prevent pre-reactions and to achieve optimum use of precursors, we will treat 75 mbar growth pressure as default in our further experiments unless otherwise specified.

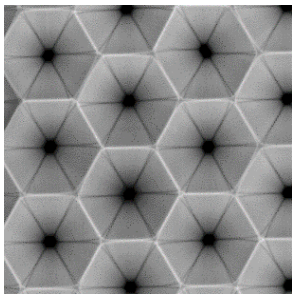

Figure 4: SEM image of Δ-type sample after growth of ~2 µm AlGaN at 75 mbar in high V/III ratio condition.

2.4 Effect of V/III ratio

Another way to reduce pre-reaction between TMAl and ammonia is through reduction of ammonia partial pressure. For this reason, but also to find whether the reduced V/III ratio changes relative growth rates between the *c*-plane and semipolar planes, this direction was chosen for further expanding of explored space of growth parameters (~3.3 times reduced ammonia flow: from 33% down to 10% of total flow). To account for the corresponding change in AlGaN composition, TMAl/TMGa ratio was once again adjusted by modifying the TMAl flow, based on separately grown planar calibration samples, to maintain aluminium content around target 20% which led to minor

shifts in the effective V/III ratio in each case. The rough V/III ratio was originally ~700 and hence around ~230 for the reduced ammonia partial pressure growth.

The effect of the reduced V/III ratio on surface morphology can be seen from Figure 5 where top view SEM images of Δ-, Δ+- and Y-type samples are presented. The following factors are noted. First of all, lower V/III ratio also favours semi-polar facet formation resulting in hexagonal V-pits rotated by 30° with respect to the wet etched μ-holes as can be observed from Figure 5, *a*. Secondly, it appears that lower V/III ratio makes it harder to preserve/recover the facet morphology of semipolar facets. This can be seen from the curvature of the border/intersection of slanted facets with *c*-plane (one of which is highlighted with a yellow curve in Figure 5, *a*). Their curved shape (rather than being a straight line) indicates a slight concavity in the horizontal direction of {11$\underline{2}$2} planes.

Despite shrinkage of *c*-plane, this process is apparently slower for regions located next to the intersections between adjacent {11$\underline{2}$2} planes. This may indicate slightly faster growth rate of semipolar facets in these regions close to their mutual intersection compared to those in the middle, which exactly defines their above-mentioned concavity. A possible mechanism defining such a behaviour is that these intersections may act as origins of easier nucleation of steps in the horizontal (lateral) direction. Note, that acceptance solid angle for precursors to land in this corner regions is smaller compared to the centres of {11$\underline{2}$2} facets and so growth rate there should be slower without lateral adatoms surface diffusion. While moderate surface diffusion in the case of high V/III ratio can only compensate for this effect so that no significant gradient is observed (Figure 4), the increased surface mobility at lower V/III ratio diminishes the difference in amount of adatoms obtained directly from the ambient while the easier nucleation of steps becomes more significant factor resulting in a locally increased growth rate.

With the reduced crystallographic quality of semipolar facets of Δ-type sample at low V/III ratio, our Δ+-type sample could not form sharp crystallographic {11$\underline{2}$2} facets (Figure 5, *b*), while it was possible at high pressure/high V/III ratio conditions (see Figure 2, *b*).

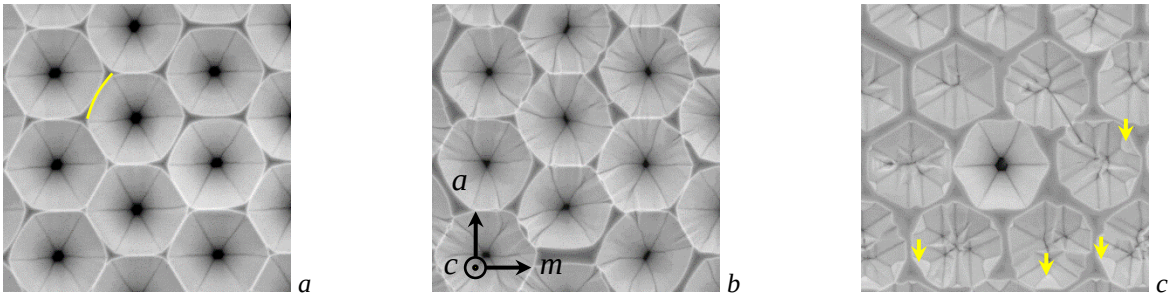

Figure 5 : SEM images of a) Δ-type b) Δ+-type c) Y-type samples after growth of ~2 µm AlGaN at low V/III ratio of ~232 and 75 mbar. Yellow arrows in figure (c) point to some of the residuals of {11$\underline{2}$2} facets.

Further consequences of the enhanced diffusion length of group-III adatoms are: a) improved non-polar growth rate due to more (mostly gallium) adatoms reaching non-polar planes inside the tunnel from the slower growing semi-polar planes, and b) enhanced parasitic growth direct on sapphire substrate at the bottom of the µ-holes. The former has manifested itself in smaller diameter of the tunnel for samples of all three types. The latter resulted in Y-type sample V-pits being filled with material grown at the bottom.

In general, due to the high 'stickiness' of aluminium species, AlGaN growth starts everywhere: at *c*-plane, at non-polar planes and even on sapphire in the bottom of µ-holes (the parasitic growth mentioned above). As growth progresses, non-polar planes expand inward forming a vertical V-pit 'tunnel' region in the middle (with its upper part being the intersection between non-polar and semipolar facets). As the V-pit tunnel shrinks, the solid angle at which the sapphire surface at the bottom of it 'sees' the ambient reduces. This leads to a decrease of the direct supply of precursors there due to *shadowing* effect[18] suppressing further parasitic growth. However, if parasitically grown material reaches the upper part of the tunnel before it is sufficiently 'closed', then shadowing is prevented allowing parasitic growth to take over, climbing up the semipolar facets. For all samples at high V/III ratio, their V-pit tunnels shrink enough before this happens because the width-to-depth aspect ratio of the initial µ-holes was optimised for that based on preliminary experiments not reported here. While for Δ/Δ+-type samples, parasitic growth is suppressed even at low V/III ratio, most of V-pit tunnels of Y-type sample does not have time to close early enough. This is due to µ-holes of the Y-type sample being of higher than critical width-to-depth aspect ratio

for these growth conditions. As seen from Figure 1, *b*-*d*, wet etched µ-holes of the Y-type sample are slightly larger laterally than those of Δ- and even Δ+-type samples while being of the same depth.

Normally, under these growth conditions, µ-holes should evolve into V-pits with *a*-plane-tilted semi-polar facets {11$\underline{2}$2} as is observed for the Δ-type sample (Figure 5, *a*). However, orientation of the semipolar facets for most of the µ-holes of the Y-type sample is ultimately *m*-plane tilted (compare to Figure 1, *d*). The generally reduced crystallographic quality of their facets is due to randomness of the undesired parasitic growth and in this regard can be ignored. Residuals of *a*-plane-tilted semi-polar facets are visible where parasitic growth did not have time to climb up all the way from the tunnel to the *c*-plane (marked with yellow arrows in (Figure 5, *c*). As an extreme example of that, one V-pit in the centre of Figure 5, *c* has no parasitic growth and so its semipolar facets are oriented as expected for these growth conditions (*a*-tilted: {11$\underline{2}$2}).

It is interesting to speculate about the crystallographic orientation of the parasitic growth and why it differs from the one dictated by growth conditions. While it is clear from the general principle that the crystallographic orientation of V-pit facets is defined by the relative growth rates of the concurring semi-polar orientations, further and more detailed analysis of this observation will be given later (subsection 2.7.1).

2.5 Effect of growth temperature

Reactor temperature defines a number of critical parameters during growth starting from ammonia cracking efficiency, and continuing to adatom diffusion lengths, desorption/decomposition rate, chemical activity of precursors and unwanted impurities. As low V/III ratio conditions (NH_3 constitutes only 10% of total flow) in general, and Δ+-type sample in particular, showed degraded crystallographic quality of µ-HC structures a temperature series of samples was grown at high V/III ratio (NH_3 constitutes 33% of total flow) and only for Δ- and Y-type samples.

The surface morphology of Δ- and Y-type samples grown at different temperatures are presented in Figure 6. From this series it is obvious that higher temperature favours coalescence as for both Δ- and Y-type samples *c*-plane area significantly increased after ~2 µm AlGaN growth. As

before, the shape of what has left of µ-holes is hexagonal with orientation 30° rotated versus its original (prior to overgrowth) orientation. Among the two concurrently grown samples Δ-type has relatively larger *c*-plane region compared to Y-type because of the initial overall larger *c*-plane area to begin with.

Conversely, low temperature growth of AlGaN results in absolute extinction of *c*-plane even in the Δ-type sample which completely loses triangular *c*-plane regions having instead pyramidal regions where *c*-plane use to be (marked with yellow triangle in Figure 6. *a*; compare to Figure 1, *b*). What is more remarkable, no rotation of the semipolar facets happens at this low temperature i.e. *m*-

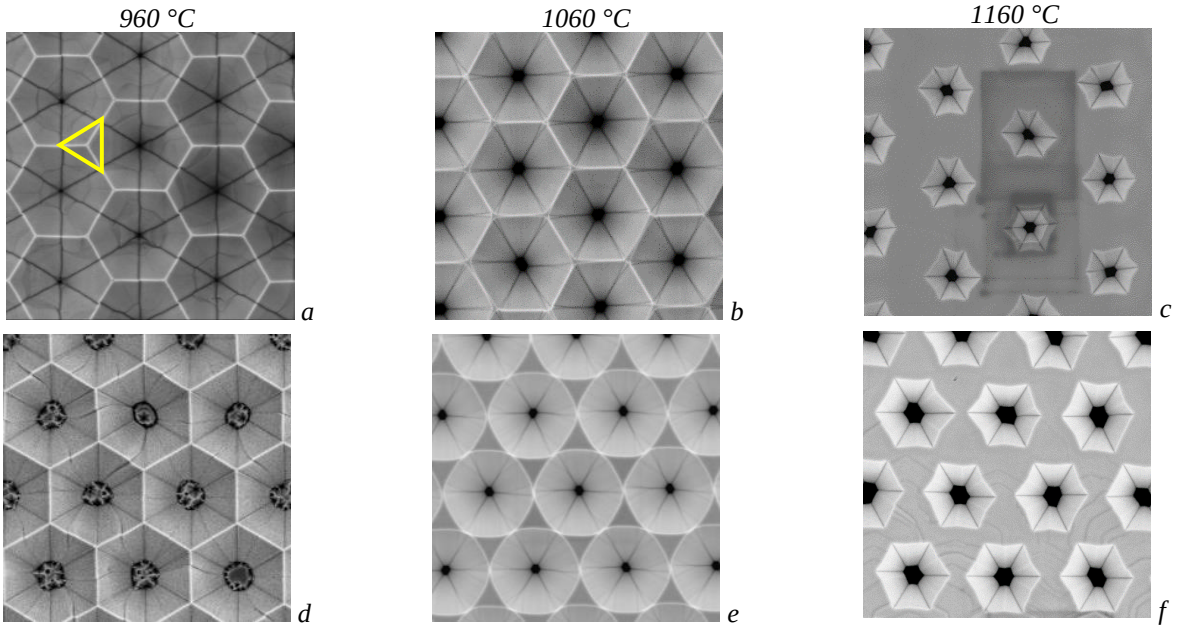

Figure 6: Top view SEM images of Δ-(a-c) and Y-type (d-f) samples after growth of ~2 µm AlGaN at high V/III ratio, 75 mbar and growth temperatures of 960°C (a, d), 1060°C (b, e), and 1160°C (c, f). Yellow triangle in figure (a) highlights a pyramidal feature.

tilted semi-polar facets (Figure 6. *a* and *d*) and not *a*-tilted are formed, so that unlike at higher temperatures Δ-type (before growth) µ-HC stays Δ-type in orientation, and similarly for the Y-type µ-HC. By tilting samples in SEM, it was possible to measure angle of the *m*-tilted facets which was found to be ~60° from which we conclude their crystallographic orientation to be {1$\underline{1}$01}. This is very common crystallographic orientation of 3D GaN nano/micro structures although those of a convex shape e.g nanocolumns[19], micro-fins[20], etc.[20]. As was speculated in section 2.2, which semipolar plane forms in the apertures is defined by their relative growth rates. From preserving the original orientation of the µ-hole hexagonal shape we can conclude that growth rate along (11$\underline{2}$2)

direction is not faster by at least ~15% ((1/cos(~30°) – 1)×100%) than that along (11̲01) direction at this growth conditions. Mutual competition of these two planes will be further discussed in one of the next sections.

While it is clear that high temperature favours coalescence, it is still interesting to understand how it will be affected by V/III ratio at the elevated temperature. For this reason, an attempt was made to prepare low V/III ratio samples, and their SEM pictures are shown below (Figure 7).

From comparison of Figure 6, *c*, *f* and Figure 7, *a*, *b*, respectively, one can see that to target coalescence, both high temperature and high V/III ratio are required. While the higher temperature seems to be able to 'cure' low V/III ratio's effect of deteriorated crystallographicity (observed in Figure 5), it is on its own cannot significantly increase *c*-plane area compared to that before growth.

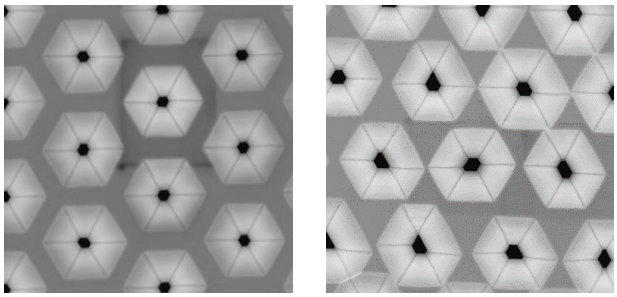

a *b*

Figure 7: Top view SEM images of (a) Δ-and (b) Y-type samples after growth of ~2 µm AlGaN at low V/III ratio, 75 mbar and growth temperatures of 1160°C.

Triangular regions of Δ-type (before growth) sample convert into Y-type regions after growth, but the overall *c*-plane area does not seem to significantly increase. For the Y-type (before growth) sample, triangular regions formed after growth have a combined area seemingly larger than that of initial Y-regions. We believe this is effect of geometry (*c*-plane expansion is easier while converting Y-regions into triangles) but further expansion of these triangular regions is expected to be much slower.

One of the possible explanations why the *c*-plane is not expanding as fast as at high V/III ratio lies in the increased group-III (mostly Ga) adatom surface diffusion, whereby adatoms diffuse from the semipolar to *c*-plane, increasing the *c*-plane growth rate (G_c) and consequently reducing the semipolar growth rate (G_{sp}). From consideration of the equation (2) inequality this means the G_{sp}/G_c ratio will decrease, making the achievement of the threshold 0.5 value for coalescence harder. Further discussion on this point as it is impacted by growth temperature will be made later (Section 2.7.3).

2.6 Effect of carrier gas.

Having identified coalescence growth condition, with the view of further expansion of explored area in the space of growth parameters, the effect of switching carrier gas from hydrogen to nitrogen was examined. It is known that nitrogen carrier gas promotes lateral growth on non-polar planes[19]; however, a pure nitrogen ambient in our experiments can lead to V-pit formation even in planar *c*-plane regions. It was found that adding ~15% of hydrogen to the nitrogen/ammonia ambient can completely suppress spontaneous V-pit formation. This mostly nitrogen-rich ambient was used to repeat our high temperature and high V/III ratio growth (Figure 8, *a*). Generally, similar *c*-plane expansion has been achieved in this N_2 rich conditions. The only noticeable difference was almost complete closure of the tunnel, which can be explained by the above mentioned improved non-polar growth rate.

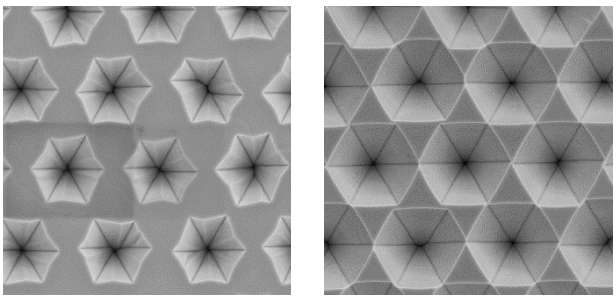

a *b*

Figure 8: SEM images of Y-type samples after growth of ~2 µm AlGaN in nitrogen rich ambient (only 15% of total flow composes H_2) at 1160°C & 75 mbar with (a) high and (b) low V/III ratios (ammonia constitutes ~33% and ~10% of total flow, respectively).

Similarly, to the pure hydrogen conditions, reduction of V/III ratio significantly slows down *c*-plane expansion.

2.7 Discussion

After having explored the growth parameter space and identifying suitable conditions favouring formation of V-pits with semi-polar {11$\underline{2}$2} facets and *c*-plane expansion (coalescence), to draw a comprehensive picture of overgrowth mechanisms, a systematic study of the surface morphology evolution at the corresponding growth conditions has been undertaken.

2.7.1 Semi-polar facet formation

From the above presented data, it is observed that at high enough temperatures initially 'nearly *m*'-plane-faceted (1$\underline{1}$00) µ-holes transform into {11$\underline{2}$2}-faceted V-pits (e.g., Figure 4, *a*). Furthermore, at sufficiently low temperatures this transformation does not occur (Figure 6. *a* and *d*).

On the other hand, a 'reverse' transformation to some form of *m*-plane-tilted semipolar facets occurs when the V-pits get infilled with parasitic growth (Figure 5, *c*). This can be seen by the 30° rotation of the facet boundaries within these pits compared to the pit in the centre of the Figure where parasitic growth did not occur. To understand these behaviours, a series of samples were grown with different nominal thicknesses (0.25 – 4 µm) in conditions (1060 °C | high V/III | 75 mbar | H_2) favouring semipolar facet formation, and the corresponding SEM images are presented in Figure 9.

In the first stages of growth, the *m*-plane-tilted semipolar planes {1$\underline{1}$01} form which is defined by the initial geometry of the µ-holes. The semipolar plane angle of ~60° was confirmed by tilted SEM analysis meaning this is the same family of planes that we observe at lower temperatures (e.g. Figure 6. *a*). Once these planes are fully developed, another semipolar plane starts to form at the intersection between adjacent {1$\underline{1}$01} planes. It is interesting to note that the intersection of two adjacent semipolar planes of {1$\underline{1}$01}-family is oriented relative to *c*-plane at an angle exactly equal to that of [11$\underline{2}$2] relative to *c*-plane. The formation of {11$\underline{2}$2} semipolar planes is visible at 0.5 µm of nominal thickness. Further (at 1 µm of nominal thickness), an even more complicated crystallographic configuration is observed: V-pits form a distinct dodecagonal shape for Δ-type sample (Figure 9, *g*) and less obvious but still recognisable octadecagonal shape for Y-type sample (Figure 9, *h*). The twelve semipolar facets in the Δ-type sample (Figure 9, *g*) are two families of semipolar planes which, assuming the angle of these facets with *c*-plane stays ≈60° (not measured) can be indexed as {12$\underline{3}$3} and {1$\underline{3}$23} as they azimuthally oriented just in between *a*- and *m*-directions. Their nonpolar versions {12$\underline{3}$0} and {1$\underline{3}$20} according GaN Wulff plot should be faster growing than even *a*-planes which 'sit' in local minima[21] while maxima correspond roughly to these two families of non-polar planes. These non-polar planes are predicted to be typical for growth of

wurtzite materials in apertures[22], and have been reported previously for wurtzite InP nanostructures[23]. So, appearance of expectedly fast-growing semipolar versions of these planes in our µ-holes is not completely surprising. In the Y-type sample, in addition to these twelve, also six residual *a*-plane-tilted {11$\underline{2}$2} are present (Figure 9, *h*), which are located next to residual triangular regions.

In the absence of data between 1 and 2 µm, it is hard to speculate about how exactly the competition between {12$\underline{3}$3}+{1$\underline{3}$23} and {11$\underline{2}$2} takes place, but the outcome is clear, at least for the Δ-type sample: the {11$\underline{2}$2} family of planes becomes dominant by the nominal thickness of 2 µm and remains dominant after another 2 µm of AlGaN growth (Figure 9, *i*, *k*)). While both {12$\underline{3}$3}- and {1$\underline{3}$23}-facets are expected to be faster growing than {11$\underline{2}$2}[21], there is an argument in favour of combination of these families of planes being less stable. There is an inherent asymmetry for these facets in terms of their mutual intersections: some of these intersections are tilted versus *c*-axis towards *m*-planes (horizontal in Figure 9, *g* and those at ±60° to them) while others are tilted

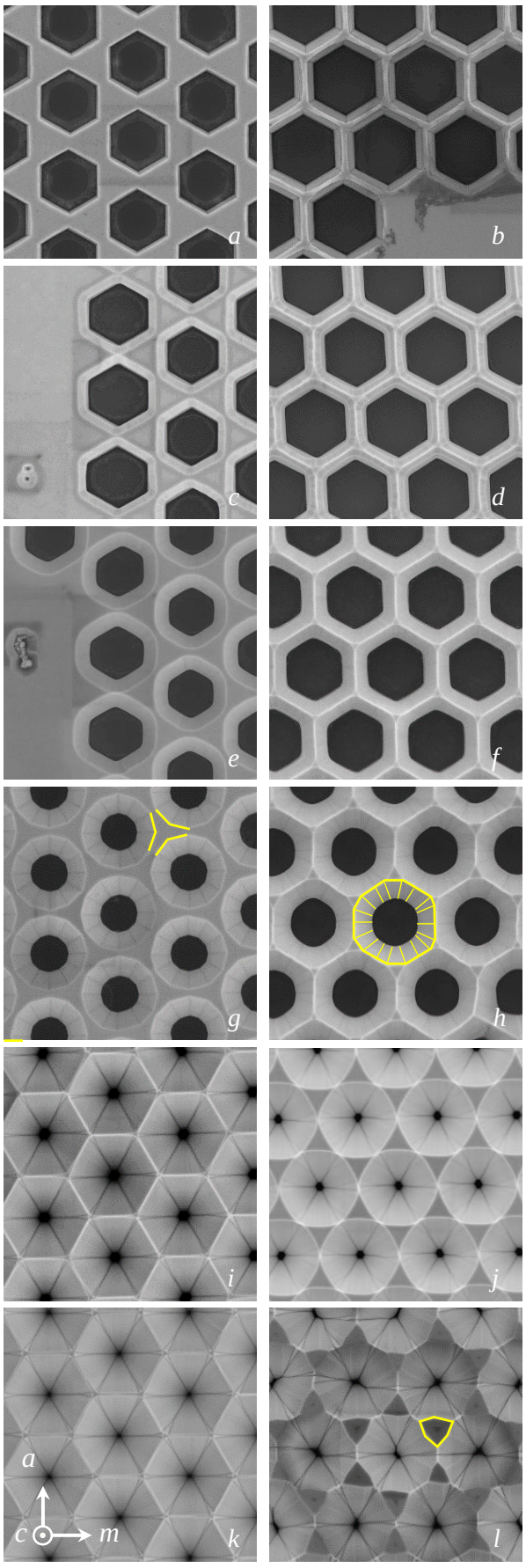

Figure 9: Surface morphology evolution of Δ- and Y-type µ-HC structures grown in conditions favouring semi-polar facet formation.

towards *a*-planes (vertical and those at ±60° to them, *ibid.*). As was discussed before, mutual intersections of semipolar facets may act as origins of growth steps, so it is logical to assume that the step-generating efficiency of intersections along *a*- and *m*-directions is significantly different (higher for those oriented along *a*-axis as it is faster growing[21]). This should lead to locally faster growth rate and gradual inclination of two neighbouring facets corresponding {11$\underline{2}$2} e.g. [32$\underline{1}$3] and [21$\underline{3}$3] towards [11$\underline{2}$2]. This is seemingly how {11$\underline{2}$2}-facets eventually reappear in Δ-type sample at nominal thicknesses of overgrowth over 1 µm.

Despite a moderate temperature of 1060°C favouring *c*-plane shrinkage for our Δ-type µ-HC sample, the Y-type (before growth) sample (Figure 9, *b*) seems to be able to develop triangular *c*-plane regions as growth progresses, whose area increases in the process of conversion of the V-pit facets from *m*-plane-tilted ({1$\underline{1}$01}) as in Figure 9, *f* , to *a*-plane-tilted ({1122}) ones, as in Figure 9, *j*. In general, this seems to be defined by the geometry of the array (after the growth, the initial Y-type HC sample effectively converted to a Δ-type one). The growth rate ratio between *a*-plane-tilted ({1122}) facets and the *c*-plane in this 1060°C case seems to be not much lower than 0.5 (cos(≈60°), see equation (2)) which allows observed flat triangular *c*-planes to form (Figure 9, *j*) as opposed to the pyramidal regions that occur in the Δ-type sample at low temperature (Figure 6, *a*).

The 'final' shape of these 'triangular' *c*-plane regions (one of which is highlighted in Figure 9, *l*) suggests that facets of the V-pits after 4 µm of nominal growth are not exactly *a*-plane tilted ({11$\underline{2}$2}) ones, but instead each of the six fundamental a-tilted facets is split into two sub-facets with slightly different crystallographic orientations. We can speculate that these belong to {12$\underline{3}$3} and {1$\underline{3}$23} families of planes already mentioned above (in the discussion concerning Figure 9, *g*). However, in this case, these sub-facets intersect with each other making the fundamental V-pit facets convex-shaped (as can be seen from comparison of highlighted shapes in Figure 9, *l* and Figure 9, *g*). It is hard to assertively conclude why the dominant crystal planes are different in Δ- and Y-type samples. One possibility is that it is something to do with the presence and absence of *c*-plane regions in the 'final' topologies, which is defined by the orientation of µ-HC array.

The final topology of the Δ-type sample (Figure 5, *a*) is still an indication that growth along (11$\underline{2}$2)-direction (*a*-plane-tilted) is more than 15% faster compared to that along (1$\underline{1}$01)-direction (*m*-plane-tilted). However, this appears to contradict the 'reverse' transformation back to a form of *m*-plane-tilted facets when parasitic growth fills the V-pits (Figure 5, *c*). To consider this further, a 45°-tilted view of the relevant sample (Figure 10) was examined. In the figure, a rare V-pit that did not get infilled is shown in the centre. One can see that while bottoms of all infilled V-pits are visible, that of the one in the centre is not (as is expected given the depth of a {11$\underline{2}$2}-faceted V-pit). From this, it is clear that the angle of the 'new *m*-plane tilted facets' to the *c*-plane is significantly smaller than that of {11$\underline{2}$2}. As the base of all the infilled (with parasitic growth) V-pits is still visible, we conclude that the angle of the infill *m*-plane-tilted facets to the *c*-plane is close to or less than 45° (our SEM tilt angle). Hence these infill *m*-plane-tilted facets cannot be {1$\underline{1}$01} that were observed at lower growth temperatures when there is no *m*-plane-tilted to *a*-plane-tilted facet transformation. We believe that these new dominant planes are *r*-plane ({1$\underline{1}$02}) in nature, whose angle with the *c*-plane is ~43°. While the competition (in terms of growth rate) between {11$\underline{2}$2} and {1$\underline{1}$01} at these high temperature growth conditions is won by the former, that is not the case when *r*-family of planes {1$\underline{1}$02} comes into play, which the parasitic growth allows. V-pits get infilled when this occurs because the growth rate of the *r*-planes is faster than that of {11$\underline{2}$2} and probably even {12$\underline{3}$3}/{1$\underline{3}$23}. Considering the exact geometry and applying a similar approach to that used to calculate the threshold growth rate ratio (equation (2)) based on schematic information in Figure 3, it is possible to show that the precise ratio between these two semi-polar plane growth rates should be at least approximately 1.391 for the observed taking over to happen (i.e. $G_{\{1\underline{1}02\}} > 1.391 \cdot G_{\{11\underline{2}2\}}$).

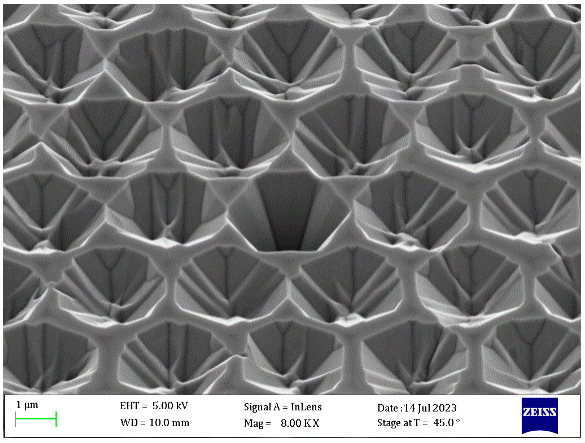

Figure 10: Tilted view SEM of the sample shown in Figure 5, c.

The reason why *r*-planes, despite being seemingly the fastest growing semipolar planes considered so far, do not dominate the surface morphology of V-pits when there is no parasitic growth is an interesting question. However, discussion of the matter would be a deviation from the main scope of this paper. Nevertheless, we provide our postulation of this in the Supplementary information.

2.7.2 Coalescence conditions:

The morphological development of the surface is under conditions favouring coalescence is shown in Figure 11. As discussed earlier for semi-polar facet conditions, initially *m*-plane tilted facets ({1$\underline{1}$01}) form. However, the formation of *a*-plane tilted facets ({11$\underline{2}$2}) starts earlier, being observable after already 0.25 µm of nominal growth, and by 0.5 µm they are dominant (Figure 11, *e*, *f*). This indicates that the competition between these two semipolar families of planes is very much in favour of {11$\underline{2}$2} one.

While in general high temperature high V/III ratio conditions favour *c*-plane expansion, things are not as trivial as they may seem at first glance. Although narrow, *c*-plane regions in our Y-type sample are present and continuous before growth (Figure 11, *d*), after 0.25 µm of nominal growth the continuity in *c*-plane disappears, and very small (and thus isolated) triangular regions form instead. Similarly, the rather large triangular regions of Δ-type sample initially shrink, while *c*-plane regions between them expand.

As was mentioned above, in a competition between *c*-plane and a semipolar plane tilted at an angle ω, for a stable topology (no *c*-plane expansion or shrinkage), the corresponding growth rates should satisfy the left part of equation (1). Since soon after the start of overgrowth two types of semipolar planes ({1$\underline{1}$01}, {11$\underline{2}$2}) coexist, the above condition applies to both families of planes separately. From what we observe (the *c*-plane shrinks opposite to *m*-plane-tilted {1$\underline{1}$01} facets, while it expands opposite to *a*-plane-tilted {11$\underline{2}$2} ones), for both semipolar planes the stability equation is not satisfied, but in different ways. For *m*-plane tilted facets $G_{0001}\cdot\cos(\omega_{\{1\underline{1}01\}}) > G_{\{1\underline{1}01\}}$ (i.e. $G_{\{1\underline{1}01\}}/G_{0001} < \cos(\omega_{\{1\underline{1}01\}})$ in contrast to expression (2) meaning coalescence is not favourable) and

$G_{0001} \cdot \cos(\omega_{\{11\underline{2}2\}}) < G_{\{11\underline{2}2\}}$ (i.e. $G_{\{11\underline{2}2\}}/G_{0001} > \cos(\omega_{\{11\underline{2}2\}})$ in accordance with expression (2) and coalescence can be favoured). From the above it is also clear that $G_{\{1\underline{1}01\}} < G_{\{11\underline{2}2\}}$, which is in line with our overall description of the growth behaviour.

Furthermore, the fast growth rate along (11$\underline{2}$2) eventually (after 2 µm of nominal growth) results in splitting of the *a*-tilted semipolar facet into two individual nearly-{11$\underline{2}$2} semipolar sub-facets (Figure 11, *i, j*), which were observed already in (Figure 9, *l*) and were identified as {12$\underline{3}$3} and {1$\underline{3}$23}. One of the possible mechanisms for that is due to the acceptance angle (solid angle at which surface receives precursors from the ambient) in the central part of an *a*-tilted semipolar plane is greater than in the regions close to the intersections of two adjacent facets while adatom surface diffusion cannot compensate for that. This process also favoured by probably faster growth rate of these intermediate (oriented azimuthally between *a*- and *m*-directions) semipolar planes compared to purely *a*-tilted {11$\underline{2}$2}. Eventually this results in change of the

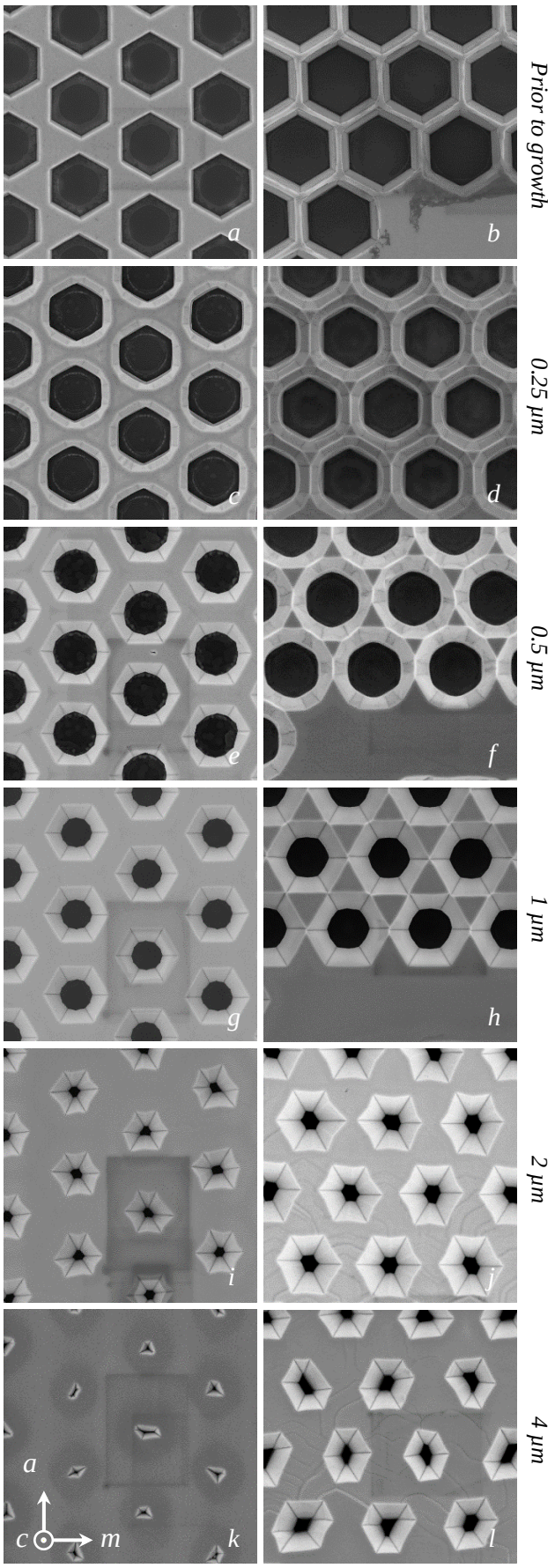

Figure 11: Surface morphology evolution of Δ- and Y-type µ-HC structures grown in condition favouring c-plane expansion.

intersection of the V-pit with the *c*-plane surface from purely hexagonal to slightly star-like shaped.

A similar evolutional behaviour was observed during the study of surface morphology as a function of thickness variation in H_2 + N_2 ambient (not shown). Coalescence in this case occurs earlier (e.g., at 4 µm of nominal growth, a full planarization of Δ-type sample has been achieved) because of, we believe, stronger lateral growth (along non-polar directions) and earlier closure of the tunnel as discussed in section 2.6. However, in terms of precursors spend there was no advantage due to higher pre-reactions and reduced growth rate compared to pure hydrogen ambient condition.

2.7.3 Possible mechanism of change in growth rate ratio

From the above discussions it is clear that the particular evolution of surface morphology is defined by the relative growth rates of the involved crystallographic orientations and the initial geometry of the µ-patterned structures. A key question is what causes these growth rates to change relatively as a function of growth condition. For example, increase in temperature seemingly enhances growth of {11$\underline{2}$2} semipolar family of planes: at low temperatures (≤ 950°C) it is so slow that no transformation (rotation) of V-pit occurs; at intermediate temperatures (~1060°C), the hexagonal shape of V-pit rotates by 30°, and finally, at high enough temperatures (≥ 1160°C), not only rotation but also coalescence takes place.

The {11$\underline{2}$2} family of planes is known to be faster growing in GaN compared to {1$\underline{1}$01} at moderate temperatures[21]. For example, Hartmann *et al.*[20] manages to grow vertical microfin structures (with only horizontal *c*- and vertical *a*-plane facets) through line apertures oriented along *m*-axis while their attempt to do the same for line apertures oriented along *a*-axis ended up in structures with pyramidal slanted facets {1$\underline{1}$01} which they explain by exactly slower growth rate along (1$\underline{1}$01). Feenstra *et al.*[24] suggested hydrogen termination of {1$\underline{1}$01} crystallographic orientation as the mechanism explaining formation of this semi-polar facets in a wide range of growth parameters. Furthermore, Akiyama *et al.*[25] studied H-termination of various III-nitride crystallographic orientations and their results show that it is possible for {11$\underline{2}$2}-planes too.

Our understanding lies in line with the above considerations: in typical MOCVD conditions, III-nitride surfaces (including *c*-plane[26]) get terminated with atomic hydrogen, which prevents group-III adatoms incorporating into the lattice. With adatoms arriving from the ambient while their incorporation is suppressed, they will accumulate on the surface increasing the adlayer thickness until their chemical potential exceeds that of hydrogen, and so the probability of adatom incorporation to the lattice increases. However, this occurs at different adlayer thicknesses for different crystallographic orientations. Thus, on complicated surfaces like our µ-HC, changes in group-III adlayer thickness occur for different facets. As a result, some facets (with thinner adlayer thickness) act as sinks of adatoms while others will effectively 'feed' them with precursors that originally arrived to them.

From our data, it is clear that over a wide range of growth conditions semipolar facets act as source of group-III adatoms while the *c*-plane acts as sink, leading to a low G_{sp}/G_c ratio, apparently below 0.5 (causing *c*-plane regions to shrink and disappear). The hydrogen chemical potential is known to decrease with temperature[27], which reduces the above mentioned adlayer thickness differences between facets, and this then appears to reduce the 'feeding' of the *c*-plane with group-III adatoms (that initially landed on the semipolar facets). This has the effect of increasing the G_{sp}/G_c ratio to about 0.5 so that *c*-plane neither expands too much nor shrinks (e.g. Figure 7). Increased ammonia flow reduces adatom surface diffusion length, which on top of the reduced adlayer thickness differences between different facets (due to high temperature) suppresses the *c*-plane 'feeding' even further, resulting in a further increase in the G_{sp}/G_c ratio, to above 0.5 and hence allows *c*-plane expansion (Figure 11).

It looks like the G_{sp}/G_c ratio increase discussed above occurs faster for the {11$\underline{2}$2}-planes leading to an initially faster growth rate compared to {1$\underline{1}$01} which leads to the 30° rotation of hexagonal V-pits and then to {11$\underline{2}$2}-planes growth rate high enough to satisfy the coalescence condition ($G_{\{11\underline{2}2\}}/G_{[0001]} > \cos(\omega_{\{11\underline{2}2\}})$). The reason for apparently stronger temperature dependence of H-termination of {11$\underline{2}$2} compared to {1$\underline{1}$01} is beyond the scope of the current study; however,

in favour of this view, two works of Hirmatsu *et al*. can be cited. They suggest that while increase of temperature leads to improved GaN growth rate along (11$\underline{2}$2) direction[28] , the same does not occur for the growth rate along (1$\underline{1}$01)[29].

3 Conclusion

In conclusion, surface morphology evolution during AlGaN overgrowth on microhoneycomb-type patterned relaxed AlGaN template has been studied. Growth conditions leading to either planarization through coalescence or vice-versa formation of ordered arrays of regular faceted V-pits have been identified. The observed behaviours are defined by relative growth rates (and their dependence on growth parameters) of different crystallographic orientations appearing during different stages of surface morphology evolution.

The exact peculiarities of surface morphology evolution can be explained from the principle that for growth in cavities (concave shapes) faster growing planes develop and slower growing ones vanish while the opposite takes place in the case of convex shapes. Despite of simplicity of the above guideline, the accurate assessment is required in the case of μ-HC as different facets can be part of concave and convex shapes simultaneously e.g., convex in the vertical direction while concave in the horizontal direction.

Our results suggest that coalescence of μ-HC patterns is defined by the growth rate of {11$\underline{2}$2} family of semipolar planes which is found to increase with temperature. Following published literature, we propose hydrogen termination of semipolar facets as the main mechanism of the reduced growth rate at wide range of growth parameters and conclude that this termination reduces with increased temperature much more rapidly for {11$\underline{2}$2} compared to {1$\underline{1}$01}.

The reported here technique may be useful in fabrication of relaxed planar AlGaN of improved crystal quality for high performance UV LEDs as well as ordered arrays of regular V-pits with crystallographic micro facets for novel type semipolar UV LEDs.

4 References

1. Kamiyama, S. *et al.* UV Light-Emitting Diode Fabricated on Hetero-ELO-Grown Al0. 22Ga0. 78N with Low Dislocation Density. *Phys. Status Solidi A* **192**, 296–300 (2002).
2. Wang, K. *Development of Crack-free AlGaN on GaN based on Facet-Controlled Epitaxial Lateral Overgrowth*. (North Carolina State University, 2020).
3. Allerman, A. A., Crawford, M. H., Lee, S. & Clark, B. Low dislocation density AlGaN epilayers by epitaxial overgrowth of patterned templates. *J. Cryst. Growth* **388**, 76–82 (2014).
4. Omori, T. *et al.* Reduction of dislocation density in lattice-relaxed Al0. 68Ga0. 32N film grown on periodical 1 μm spacing AlN pillar concave-convex patterns and its effect on the performance of UV-B laser diodes. *Appl. Phys. Express* **15**, 031004 (2022).
5. Kueller, V. *et al.* Growth of AlGaN and AlN on patterned AlN/sapphire templates. *J. Cryst. Growth* **315**, 200–203 (2011).
6. Zhang, J. *et al.* Crack-free thick AlGaN grown on sapphire using AlN/AlGaN superlattices for strain management. *Appl. Phys. Lett.* **80**, 3542–3544 (2002).
7. Iwaya, M. *et al.* Reduction of etch pit density in organometallic vapor phase epitaxy-grown GaN on sapphire by insertion of a low-temperature-deposited buffer layer between high-temperature-grown GaN. *Jpn. J. Appl. Phys.* **37**, L316 (1998).
8. Scholz, F. *et al.* Studies on defect reduction in AlGaN heterostructures by integrating an in-situ SiN interlayer. *Jpn. J. Appl. Phys.* **52**, 08JJ07 (2013).
9. Kneissl, M., Rass, J., & others. III-Nitride ultraviolet emitters. *Springer Series in Materials Science* (2016).
10. Iwaya, M. *et al.* High-Efficiency GaN/AlxGa1—xN Multi-Quantum-Well Light Emitter Grown on Low-Dislocation Density AlxGa1—xN. *Phys. Status Solidi A* **188**, 117–120 (2001).
11. Karpov, S. Y. & Makarov, Y. N. Dislocation effect on light emission efficiency in gallium nitride. *Appl. Phys. Lett.* **81**, 4721–4723 (2002).

12. Takeda, K. *et al.* Internal quantum efficiency of GaN/AlGaN-based multi quantum wells on different dislocation densities underlying layers. *Phys. Status Solidi C* **7**, 1916–1918 (2010).

13. Pernot, C. *et al.* Development of high efficiency 255–355 nm AlGaN-based light-emitting diodes. *Phys. Status Solidi A* **208**, 1594–1596 (2011).

14. Iwaya, M. *et al.* Suppression of phase separation of AlGaN during lateral growth and fabrication of high-efficiency UV-LED on optimized AlGaN. *J. Cryst. Growth* **237**, 951–955 (2002).

15. Amano, H., Akasaki, I., Hiramatsu, K., Koide, N. & Sawaki, N. Effects of the buffer layer in metalorganic vapour phase epitaxy of GaN on sapphire substrate. *Thin Solid Films* **163**, 415–420 (1988).

16. Liu, Z. *et al.* Micro-light-emitting diodes based on InGaN materials with quantum dots. *Adv. Mater. Technol.* **7**, 2101189 (2022).

17. Ubukata, A. *et al.* High growth rates of AlN and AlGaN on 8 ″silicon wafer using metal-organic vapor phase epitaxy reactor. *Phys. Status Solidi C* **10**, 1353–1356 (2013).

18. Adhikari, S. *et al.* Nonpolar Al x Ga1- x N/Al y Ga1- y N multiple quantum wells on GaN nanowire for UV emission. *Nano Res.* **15**, 7670–7680 (2022).

19. Zubialevich, V. Z., Pampili, P. & Parbrook, P. J. Thermal stability of crystallographic planes of GaN nanocolumns and their overgrowth by metal organic vapor phase epitaxy. *Cryst. Growth Des.* **20**, 3686–3700 (2020).

20. Hartmann, J. *et al.* High aspect ratio GaN fin microstructures with nonpolar sidewalls by continuous mode metalorganic vapor phase epitaxy. *Cryst. Growth Des.* **16**, 1458–1462 (2016).

21. Leung, B., Sun, Q., Yerino, C. D., Han, J. & Coltrin, M. E. Using the kinetic Wulff plot to design and control nonpolar and semipolar GaN heteroepitaxy. *Semicond. Sci. Technol.* **27**, 024005 (2012).

22. De Donno, M., Albani, M., Bergamaschini, R. & Montalenti, F. Phase-field modeling of the morphological evolution of ringlike structures during growth: Thermodynamics, kinetics, and template effects. *Phys. Rev. Mater.* **6**, 023401 (2022).

23. Wang, N. *et al.* Shape engineering of InP nanostructures by selective area epitaxy. *ACS Nano* **13**, 7261–7269 (2019).

24. Feenstra, R. M., Dong, Y., Lee, C. & Northrup, J. Recent developments in surface studies of GaN and AlN. *J. Vac. Sci. Technol. B Microelectron. Nanometer Struct. Process. Meas. Phenom.* **23**, 1174–1180 (2005).

25. Akiyama, T., Seta, Y., Nakamura, K. & Ito, T. Modified approach for calculating individual energies of polar and semipolar surfaces of group-III nitrides. *Phys. Rev. Mater.* **3**, 023401 (2019).

26. Van de Walle, C. G. & Neugebauer, J. Role of hydrogen in surface reconstructions and growth of GaN. *J. Vac. Sci. Technol. B Microelectron. Nanometer Struct. Process. Meas. Phenom.* **20**, 1640–1646 (2002).

27. Van de Walle, C. G. & Neugebauer, J. First-principles surface phase diagram for hydrogen on GaN surfaces. *Phys. Rev. Lett.* **88**, 066103 (2002).

28. Hiramatsu, K. *et al.* Fabrication and characterization of low defect density GaN using facet-controlled epitaxial lateral overgrowth (FACELO). *J. Cryst. Growth* **221**, 316–326 (2000).

29. Hiramatsu, K. *et al.* Recent progress in selective area growth and epitaxial lateral overgrowth of III-nitrides: effects of reactor pressure in MOVPE growth. *Phys. Status Solidi A* **176**, 535–543 (1999).